

## Electronic Supplementary Information (ESI) for

# Topology-dependent hydrocarbon transformations in the methanol to hydrocarbons reaction studied by *operando* UV-Raman spectroscopy

*Matteo Signorile<sup>a\*</sup>, Daniel Rojo-Gama<sup>b,c</sup>, Francesca Bonino<sup>a</sup>, Pablo Beato<sup>b\*</sup>, Stian Svelle<sup>c</sup>,*

*Silvia Bordiga<sup>a</sup>*

<sup>a</sup> Department of Chemistry, NIS and INSTM Reference Centre, Università di Torino, Via G. Quarello 15, I-10135 and Via P. Giuria 7, I-10125, Turin, Italy

<sup>b</sup> Haldor Topsøe A/S, Haldor Topsøes Allé 1, 2800 Kgs. Lyngby, Denmark

<sup>c</sup> Center for Materials Science and Nanotechnology (SMN), Department of Chemistry, University of Oslo, P.O. Box 1033, Blindern, N-0315 Oslo, Norway

### Corresponding authors:

\* Matteo Signorile, [matteo.signorile@unito.it](mailto:matteo.signorile@unito.it)

\* Pablo Beato, [pabb@topsoe.com](mailto:pabb@topsoe.com)

## 1. Key characterization and catalytic performances data for the five zeolite catalysts

Table S1. Key characterization data for the five zeolite catalysts from ref. 1: BET surface area (and its external surface component), pores volume (and its micropores fraction), average particle size and shift of the Brønsted O–H stretching mode ( $\Delta\nu(\text{OH})$ ) upon CO adsorption at 77K.

Sample	Si/Al	BET area (m <sup>2</sup> g <sup>-1</sup> )	External area (m <sup>2</sup> g <sup>-1</sup> )	Total pore volume (cm <sup>3</sup> g <sup>-1</sup> )	Micropore volume (cm <sup>3</sup> g <sup>-1</sup> )	Particle size (μm)	$\Delta\nu(\text{OH})$ upon CO adsorption (cm <sup>-1</sup> )
ZSM-5	15	414	5	0.18	0.17	1 - 4	328
Beta	17	677	190	0.99	0.19	<1	311
Mordenite	8	498	4	0.19	0.19	2 - 6	310
ZSM-22	47	232	12	0.08	0.08	2 - 5	323
SAPO-34	11	708	5	0.34	0.27	<1	277

Table S2. Key catalytic performance data for the five zeolite catalysts from ref. 1: times on stream at which MeOH conversion drops to 50% ( $t_{0.5}$ ), conversion capacities ( $R_0$ , derived from the Janssens model)<sup>2</sup> and deactivation coefficients (a).

Sample	$t_{0.5}$ (h)	$R_0$ (mol <sub>MeOH</sub> mol <sub>acid site</sub> <sup>-1</sup> )	a (g <sub>cat</sub> mol <sub>MeOH</sub> <sup>-1</sup> )
ZSM-5	11	1415	0.2
Beta	6.5	898	0.3
Mordenite	0.5	64	4.0
ZSM-22	1.4	491	1.3
SAPO-34	13.3	1136	0.1

## 2. UV-Raman spectra of additional reference compounds

In Figure S1 some compounds useful in the operando experiments interpretation are reported.

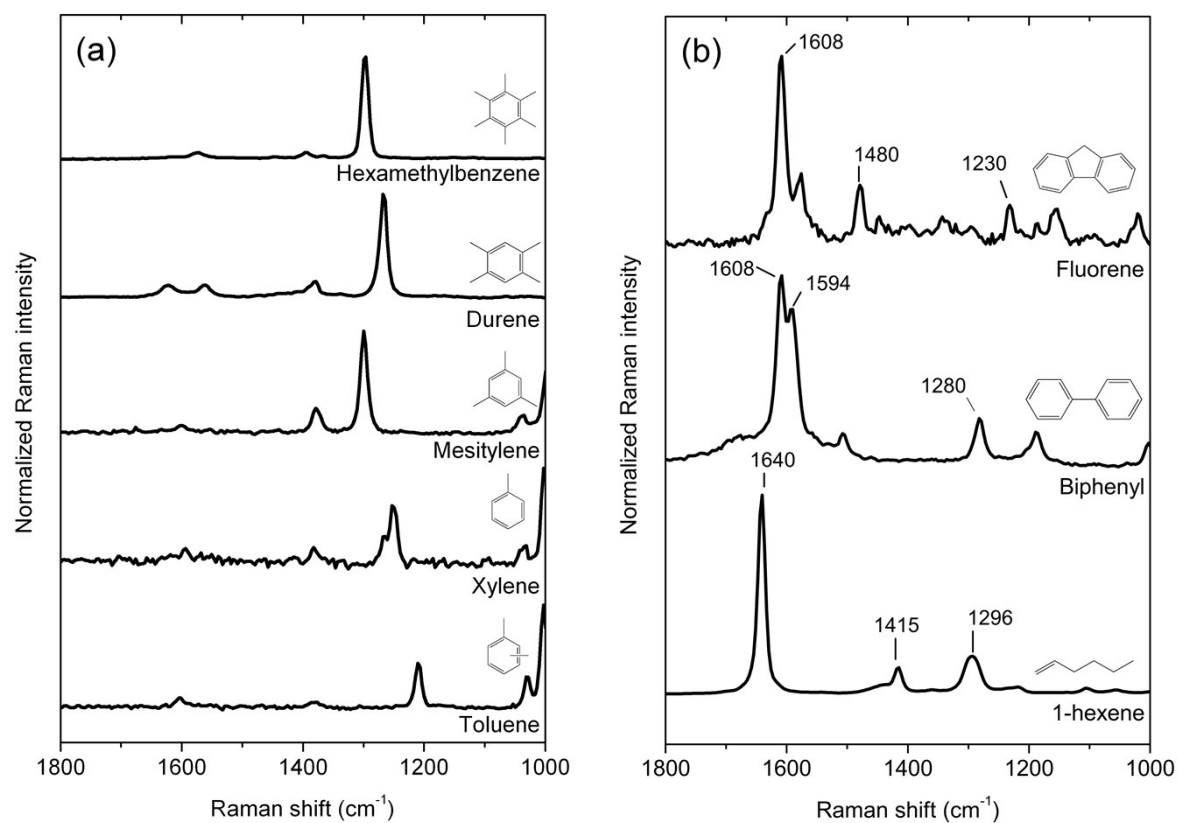


Figure S1. UV-Raman (244 nm) spectra of: a) methylated benzenes; and b) other useful compounds.

The spectra have been acquired according to the experimental procedure previously described for polycyclic aromatic compounds.<sup>3</sup>

### 3. Simulation of the Raman spectra of selected methylated PAHs

Since their unavailability for measurements, the Raman spectra of some compounds of interest were simulated. The focus was in particular on the effect of methylation over the skeletal vibrational modes of PAHs: naphthalene, anthracene and phenanthrene were selected as representative model since their affordable computational cost. Calculation were performed with the Gaussian09 code (D03 release)<sup>4</sup> at the B3LYP hybrid functional computational level,<sup>5,6</sup> including dispersive forces according to the Grimme D3 scheme.<sup>7</sup> The TZV2P basis set from Ahlrichs was exploited on C atoms, whereas a Pople's 6-311++G(2d,2p) described H atoms.<sup>8,9</sup> The "ultrafine" pruned integration grid (99 radial shells and 590 angular points per shell) was chosen to guarantee a good numerical precision necessary for a proper description of the flexible methyl groups. Each molecule was geometry relaxed, then a frequency calculation was performed. In order to better estimate the UV-Raman intensities (i.e. trying to account for resonance), the dynamic CPHF evaluation of Raman intensities was performed. The excitation energy was calibrated on the basis of the electronic transitions computed for the bare naphthalene, anthracene and phenanthrene molecules through TD-DFT. The discrepancy between simulated and experimental electronic transition wavelength was determined to be in average -12 nm. Thereby, the excitation wavelength in dynamic CPHF was set to 232 nm to simulate the experimentally exploited 244 nm excitation. The simulated vibrational frequencies have been scaled through the following linear relation, derived from the linear fitting of the  $\nu_{\text{exp}}$  vs  $\nu_{\text{calc}}$ :

$$\nu_{\text{calc,scaled}} = 4.86 + 0.97 \cdot \nu_{\text{calc}}$$

The simulated Raman spectra of single methylated naphthalenes, anthracenes and phenanthrenes are reported in Figure S2.

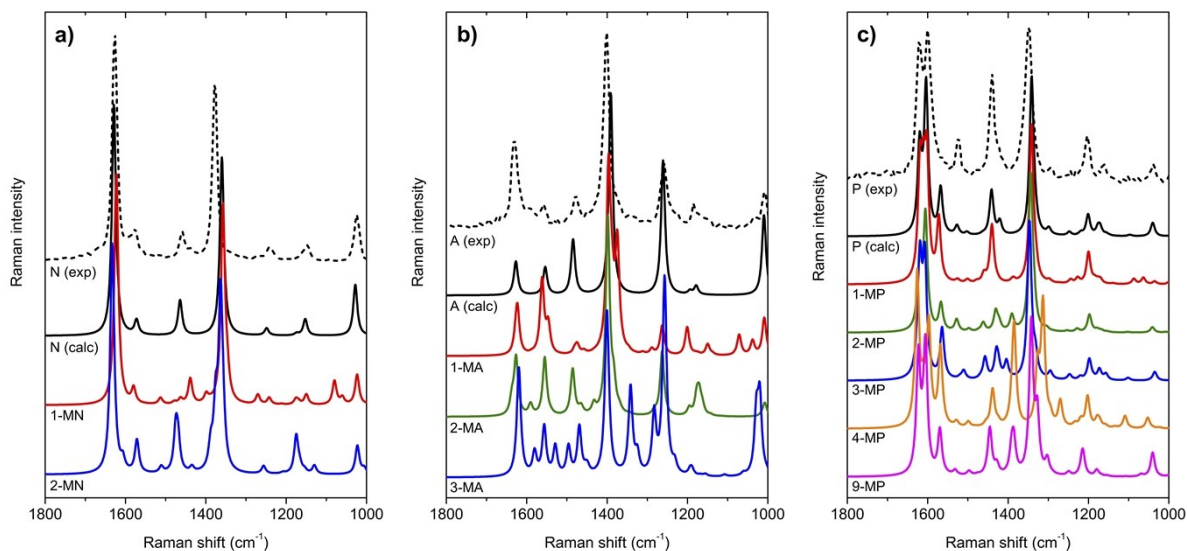


Figure S2. Calculated Raman spectra of a) bare naphthalene (N (calc)), 1-methyl-naphthalene (1-MN), 2-methyl-naphthalene (2-MN); b) bare anthracene (A (calc)), 1-methyl-anthracene (1-MA), 2-methyl-anthracene (2-MA), 9-methyl-anthracene (9-MA); and c) bare phenanthrene (P (calc)), 1-methyl-phenanthrene (1-MP), 2-methyl-phenanthrene (2-MP), 3-methyl-phenanthrene (3-MP), 4-methyl-phenanthrene (4-MP) and 9-methyl-phenanthrene (9-MP). Raman intensities have been computed through a dynamic CPHF approach simulating the 244 nm excitation. The experimental spectra ( $\lambda = 244$  nm) of naphthalene (N (exp)), anthracene (A (exp)) and phenanthrene (P (exp)) are reported for comparison. All the spectra are normalized to the maximum intensity peak for sake of visualization.

As demonstrated in Figure S2, a good agreement in terms of frequency is observed for the experimental and calculated spectra of the bare molecules, testifying the reliability of the computational approach. The dynamic CPHF approach, even being a rough approximation to the description of Raman resonance, is able to give a realistic result in term of intensities. Considering the effect of methylation of PAHs, simulation demonstrates as the high frequency region (above  $1400\text{ cm}^{-1}$ ) is slightly affected by the insertion of methyl groups in terms of peaks shift. Some variations in the relative intensities of these peaks are observed, however never resulting in a complete quench of the most intense modes. Conversely most of the spectral alterations involve the low frequency region ( $1200\text{-}1400\text{ cm}^{-1}$ ), where each molecule exhibits its vibrational fingerprints as a consequence of the different methylation.

## 4. Full MS data

Figure S3 shows the full MS charts for the five operando experiments reported in this work. The following signals/molecules have been monitored (in brackets, their  $m/z$  ratio): methanol (31), dimethylether (45), ethylene (27), propylene (and higher alkenes) (41), xylene (representative for aromatics) (91). The sudden jumps observed in the MS signals in some cases (e.g. Beta, panel b) are ascribed to the loss of fluidization, who altered the flow outgoing the reactor until restored.

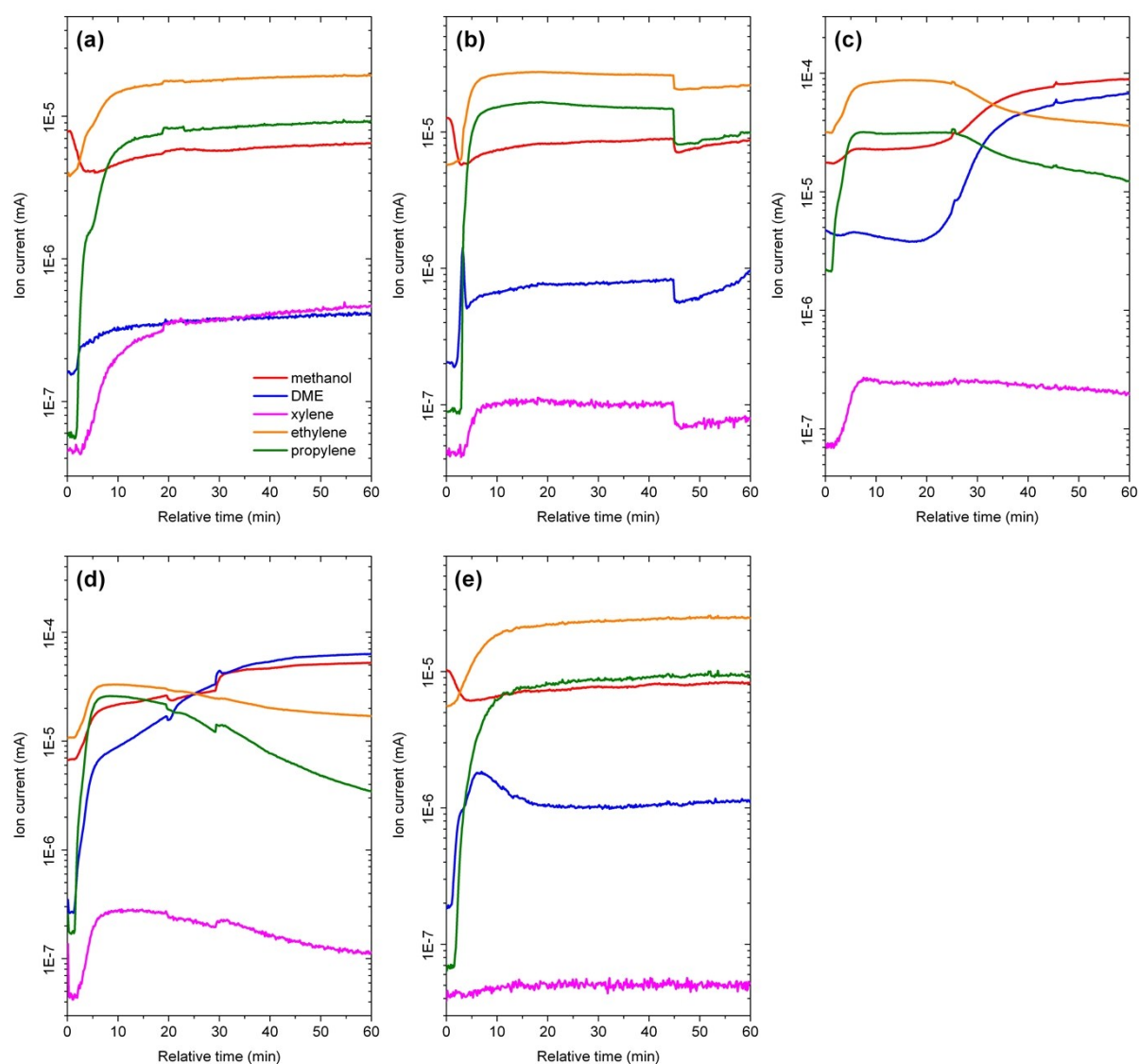


Figure S3. MS charts of the products stream analysis for: a) ZSM-5; b) Beta; c) Mordenite; d) ZSM-22; and e) SAPO-34, collected during the Raman experiments.

## SI References

- 1 D. Rojo-Gama, M. Signorile, F. Bonino, S. Bordiga, U. Olsbye, K. P. Lillerud, P. Beato and S. Svelle, Structure–deactivation relationships in zeolites during the methanol-to-hydrocarbons reaction: Complementary assessments of the coke content, *J. Catal.*, 2017, **351**, 33–48.
- 2 T. V. W. Janssens, A new approach to the modeling of deactivation in the conversion of methanol on zeolite catalysts, *J. Catal.*, 2009, **264**, 130–137.
- 3 M. Signorile, F. Bonino, A. Damin and S. Bordiga, In Situ Resonant UV-Raman Spectroscopy of Polycyclic Aromatic Hydrocarbons, *J. Phys. Chem. C*, 2015, **119**, 11694–11698.
- 4 M. J. Frisch, G. W. Trucks, H. B. Schlegel, G. E. Scuseria, M. A. Robb, J. R. Cheeseman, G. Scalmani, V. Barone, B. Mennucci, G. A. Petersson, H. Nakatsuji, M. Caricato, X. Li, H. P. Hratchian, A. F. Izmaylov, J. Bloino, G. Zheng, J. L. Sonnenberg, M. Hada, M. Ehara, K. Toyota, R. Fukuda, J. Hasegawa, M. Ishida, T. Nakajima, Y. Honda, O. Kitao, H. Nakai, T. Vreven, J. A. Montgomery Jr, J. E. Peralta, F. Ogliaro, M. J. Bearpark, J. Heyd, E. N. Brothers, K. N. Kudin, V. N. Staroverov, R. Kobayashi, J. Normand, K. Raghavachari, A. P. Rendell, J. C. Burant, S. S. Iyengar, J. Tomasi, M. Cossi, N. Rega, N. J. Millam, M. Klene, J. E. Knox, J. B. Cross, V. Bakken, C. Adamo, J. Jaramillo, R. Gomperts, R. E. Stratmann, O. Yazyev, A. J. Austin, R. Cammi, C. Pomelli, J. W. Ochterski, R. L. Martin, K. Morokuma, V. G. Zakrzewski, G. A. Voth, P. Salvador, J. J. Dannenberg, S. Dapprich, A. D. Daniels, Å. Farkas, J. B. Foresman, J. V. Ortiz, J. Cioslowski and D. J. Fox, Gaussian 09 Revision D.03, *Gaussian 09 Revis. D.03*.
- 5 A. D. Becke, A new mixing of Hartree–Fock and local density-functional theories, *J. Chem. Phys.*, 1993, **98**, 1372–1377.

- 6 C. Lee, W. Yang and R. G. Parr, Development of the Colle-Salvetti correlation-energy formula into a functional of the electron density, *Phys. Rev. B*, 1988, **37**, 785–789.
- 7 S. Grimme, J. Antony, S. Ehrlich and H. Krieg, A consistent and accurate ab initio parametrization of density functional dispersion correction (DFT-D) for the 94 elements H-Pu, *J. Chem. Phys.*, 2010, **132**, 154104 1-19.
- 8 A. Schäfer, C. Huber and R. Ahlrichs, Fully optimized contracted Gaussian basis sets of triple zeta valence quality for atoms Li to Kr, *J. Chem. Phys.*, 1994, **100**, 5829–5835.
- 9 R. Krishnan, J. S. Binkley, R. Seeger and J. A. Pople, Self-consistent molecular orbital methods. XX. A basis set for correlated wave functions, *J. Chem. Phys.*, 1980, **72**, 650–654.